Temperature dependence of Peierls-Hubbard Phase Transition in $[Pd(cptn)_2Br]Br_2$ Studied by Scanning Tunneling Microscopy

Y. Hosomi[1], S. Yoshida[1], A. Taninaka[1], T. Yoshida[2], S. Takaishi[2], O. Takeuchi[1],

M. Yamashita[2], and H. Shigekawa[1*]

[1]*Faculty of Pure and Applied Sciences, University of Tsukuba,*
Tsukuba, 305-8573, Japan

[2]*Department of chemistry, Tohoku University, Sendai, 980-8579, Japan*

E-mail: hidemi@ims.tsukuba.ac.jp

The temperature dependence of the Peierls-Hubbard phase transition in $[Pd(cptn)_2Br]Br_2$ (cptn: 1R, 2R-diaminocyclopentane) was directly observed using a low-temperature scanning tunneling microscope. A short ligand without alkyl chains was used to form a rigid crystal lattice to reduce the effect of structural changes in the crystal with the temperature. The hysteresis in the temperature dependence of the ratio between the areas of the charge density wave (CDW) state produced by the Pd^{II}–Pd^{IV} mixed-valence state and the Mott-Hubbard (MH) state with a Pd^{III}-averaged valence state, a characteristic of the first-order phase transition, was directly observed at the atomic scale. Pinning of the CDW phase by defects was observed below the critical temperature, suggesting the growth of the CDW phase with defects as nuclei.

* corresponding author: Hidemi Shigekawa

1. Introduction

Low-dimensional materials have been extensively studied because of their novel physical properties, for example, in strongly correlated electron systems and π-conjugate systems. Among these materials, quasi-one-dimensional (quasi-1D) halogen-bridged complexes (MX chains), in which isolated one-dimensional (1D) electron systems are composed of d_{z^2}-orbitals of metal ions (M) and p_z-orbitals of bridging halide ions (X) in M–X–M–X– linear chain structures, have been attracting considerable attention owing to the strong Coulomb interaction observed in phenomena such as resonance Raman spectra[1~4] and spin-Peierls transitions[5]. While more than 300 species of quasi-1D organic complexes have been synthesized, mainly using Ni or Pt metal ions, that exhibit mixed valence states, it has been theoretically predicted that a compound complex with Pd metal will undergo a charge transfer phase transition owing to the strong competition between the energies of the electron–phonon interaction (S) and the on-site Coulomb repulsion (U), i.e., the transfer integral (T)[6~10]. This is a characteristic of the Pd compounds and called the Peierls-Hubbard phase transition and has recently been experimentally confirmed using $[Pd(en)_2Br](C_5\text{-}Y)_2 \bullet H_2O$ (en = ethylenediamine; C_5-Y = dipentylsulfosuccinate), which exhibits the phase transition between the CDW and MH states at 205 K[11].

Pd-MX chains form an M^{II}–M^{IV} mixed-valence state at room temperature, where the bridging halide ions are displaced from the midpoints between two neighboring metal ions as shown in Fig. 1(a). M^{II} and M^{IV} denote divalent and quadrivalent metals, respectively. The structure shown in Fig. 1(a) is the charge density wave produced by the strained 1D structure (Peierls deformation) caused by a large S value, which forms twofold periodicity. On the other hand, at a low temperature, an M^{III}-averaged valence state, the so-called Mott-Hubbard (MH) state, is formed owing to the large value of U, in which the bridging halogens are located at the midpoints between two neighboring metal ions without modulation, as shown in Fig. 1(b). The d_{z^2} bands of Pd^{II} and Pd^{IV} in the CDW state form a conduction band and valence band, respectively[12], while the d_{z^2} band of Pd^{III} in the MH state splits into the unoccupied upper Hubbard band (UH) and the occupied lower Hubbard band (LH), owing to the strong interaction between electrons.

The phase transition associated with the structural change shown in Fig. 1 has been experimentally observed by methods such as infrared (IR) spectroscopy, X-ray diffraction, and scanning tunneling microscopy (STM)[11]. Although these studies revealed the details of the phase transition, they were carried out for Pd complexes including ligands with long alkyl groups. For the sample with a long alkyl chain, a larger change in the Pd-Pd distance

in the b-axis direction with temperature is considered to affect the study of the characteristics around the critical temperature. [6~10, 13,14].

Here, we present the first results of STM observation of the temperature dependence of the structural change of CDW-MH phases ~~transition~~ in $[Pd(cptn)_2Br]Br_2$ (cptn: 1R, 2R-diaminocyclopentane). A sample with a short ligand without alkyl chains was used in our experiment to form a rigid crystal lattice to reduce the effect of structural changes in the crystal with temperature.

2. Experimental

Figure 2 shows the crystal structure of $[Pd(cptn)_2Br]Br_2$, an octahedral structure consisting of four N atoms (two ligands) and two Br atoms placed around a Pd atom, in which the d_{z^2} and $d_{x^2-y^2}$ orbitals respectively extend vertically along the b-axis and in the four side directions. The d_{z^2} orbital of Pd and the p_z orbital of Br strongly overlap and are alternately ordered to form a quasi-1D halogen-bridged complex.

The $[Pd(cptn)_2Br]Br_2$ crystal has a unit cell of a = 2.39 nm, b = 0.707 nm, and c = 0.529 nm, which develops twofold periodicity along the b-axis in the CDW phase, and can be directly observed by STM[14-22].

Single-crystal $[Pd(cptn)_2Br]Br_2$ samples were grown by the electrochemical oxidation method[23], which were cut and fixed on a sample stage with carbon paste. Experiments were carried out using an Omicron low-temperature scanning tunneling microscope with a base pressure of 10^{-9} Pa. The performance of a piezo scanner at low temperatures was calibrated using a Si(001) surface structure. Measurement below 100 K was not possible in our experiment because of the difficulty of making the microscope tip approach the sample owing to the large decrease in the conductivity in the MH state. In addition, when a negative bias voltage was applied to the sample, the sample surface was damaged, which may have been caused by the reduced number of carriers in the surface region of the sample. Although the details are not yet clear, all measurements reported in this paper were carried out with a positive bias voltage applied to the sample.

The sample temperature, which was measured by a thermocouple attached to the sample stage, was controlled using a resistive heater attached near the sample stage, which was cooled by liquid N_2. Thermal drift was reduced by keeping the sample at each temperature for a sufficient time before measurements, which varied from several hours to overnight depending on the conditions.

3. Results and discussion

Figure 3 shows typical STM images of the $[Pd(cptn)_2Br]Br_2$ b-c plane obtained at (a) room temperature (RT) and (b) 103 K, where the Pd atoms shown in Fig. 2 are imaged as bright spots similarly to in a previous paper[11,14]. Cross sections along the blue lines in the STM images are shown together, where L and R show the positional relationship. As shown in Fig. 3, the periodicities along the b- and c-axes are (a) (0.98 nm, 0.68 nm) and (b) (0.49 nm, 0.69 nm), respectively. Since the STM image showing the twofold periodicity is similar to that obtained at RT in a previous paper and the original periodicity appeared at lower temperature, as expected, we attributed those structures to the Pd^{II}–Br–Pd^{IV} CDW state at RT and the Pd^{III}–Br–Pd^{III} MH state at 103 K, respectively. The bright protrusions were attributed to the Pd d_{z^2} orbital, similarly to those in the previous image obtained at RT.

Next, we directly observed the temperature dependence of the phase transition. Figure 4 shows the change in the STM images of the $[Pd(cptn)_2Br]Br_2$ b-c plane with decreasing ((a) to (c)) and increasing ((d) and (e)) temperature. The area ratios between the CDW and MH phases shown above the STM images were obtained from the average of the STM images measured over 25 nm × 25 nm areas at different locations at each temperature. First, the temperature was stabilized at 155 K by adjusting the current of the heater and the required images were taken. Then the temperature was decreased to 113 K and 103 K and then increased to 115 K and 158 K in a stepwise manner by changing the current of the heater, and the images were taken at each temperature. Thermal drift was minimized by keeping the sample at each temperature for a sufficient time before measurements, as described above, which also ensured accurate temperature control. Cross sections along the lines in the STM images are shown together.

As shown in Figs. 4(a) and 4(e), almost the entire surface was occupied by the 2×1 CDW phase at 155 K, while, as shown in Fig. 4(c), almost the entire surface was covered by the MH state at 103 K; the CDW/MH area ratio was 1:9, confirming that the CDW phase and MH phase appear at high and low temperature, respectively. Here, the CDW phase, comprising ~1/10 of the surface area at 103 K and 115 K was observed around the defects, as shown in Figs. 4(c) and 4(d). Figure 4(f) shows a cross section along the 1D chain of Pd atoms surrounded by the dashed rectangle in the left of Fig. 4(d), where only one defect exists in the chain, showing the gradual change in the structure from the CDW phase near the defect located near letter L (bottom left) to the MH phase along the chain (L-R). These results suggest that the CDW phase tends to be pinned by defects at low temperatures and grows with increasing temperature. As shown in Figs. 4(c) and 4(d), the effect of defects on

the neighboring chains looks weak, which, however, may affect the critical temperature. This effect may be due to the strain around the defects, although it has not yet been confirmed.

Another noteworthy point is that the CDW/MH area ratio around 115 K was different between the surfaces observed upon the temperature being decreased ((b) 113 K, 6:4) and increased ((e) 115 K, 1:9), i.e., although the latter temperature is slightly higher, the ratio of the CDW phase is lower. The MH state remains upto a higher temperature when the temperature is increased. The hysteresis, which is a characteristic of the first-order phase transition and was observed in a previous work by macroscopic methods such as Raman spectroscopy[11], was directly observed at the atomic scale for the first time.

As reported in a previous paper, the Pd-Pd distance in the b-axis direction becomes closer for a sample with a longer alkyl chain, which increases critical temperature by ~30 K when one C atom in the alkyl chain is added[13]. As expected, the critical temperature of ~100 K observed in this experiment for the sample without alkyl chains is lower than that observed for $[Pd(en)_2Br](C_5\text{-}Y)_2 \bullet H_2O$ (en = ethylenediamine; C_5-Y = dipentylsulfosuccinate) of, 205 K[13], which is of a similar order despite their structures being different from each other. Theoretical calculations are necessary to obtain further understanding of these results. The analysis of the growth of the CDW phase in the intermediate state is important to clarify the details of the phase transition, such as the interactions in the 1D chains and between the 1D chains. The analysis of the fluctuations of the two phases and the effect of alkyl chains will also be an interesting topic. These analyses are under consideration.

4. Conclusions

We succeeded in the direct observation by STM of the phase transition between the CDW and MH phases in $[Pd(cptn)_2Br]Br_2$, in which a short ligand without alkyl chains was used to form a rigid crystal lattice to reduce the effect of structural changes with the temperature. The hysteresis in the temperature dependence of the ratio between the CDW and MH phase areas, a characteristic of the first-order phase transition, was directly observed at the atomic scale. Pinning of the CDW phase by defects was observed below the critical temperature, suggesting the growth of the CDW phase with defects as nuclei.

Acknowledgments

H.S. acknowledges the support from Japan Society for the Promotion of Science (Grant-in-Aid for Scientific Research, 15H05734).

References

1) R. J. H. Clark, M. L. Franks and W. R. Trumble, Chem. Phys. Lett., 41, 287 (1976).
2) R. J. H. Clark, M. Kurmoo, D. N. Mountney and H. Toftlund, J. Chem. Soc., Dalton Trans., 1982, 1851 (1982).
3) R. J. H. Clark, Chem. Soc. Rev. 19, 107 (1990).
4) R. J. H. Clark, Adv. Infrared Raman Spectrosc. 11, 95 (1983).
5) S. Takaishi, Y. Tobu, H. Kitagawa, A. Goto, T. Shimizu, T. Okubo, T. Mitani and R. Ikeda, J. Am. Chem. Soc. 126, 1614 (2004).
6) K. Nasu, J. Phys. Soc. Jpn. 52, 3865 (1983).
7) S. M. Weber- Milbrodt, J. T. Gammel, A. R. Bishop and E. Y. Lor, Jr., Phys. Rev. B: Condens. Matter. 45, 6435 (1992).
8) K. Iwano and K. Nasu, J. Phys. Soc. Jpn. 61, 1380 (1992).
9) D. Baeriswyl and A. R. Bishop, J. Phys. C: Solid State Phys. 21, 339 (1988).
10) A. Mishima and K. Nasu, Phys. Rev. B: Condens. Matter. 40, 5593 (1989).
11) M. Yamashita and S. Takaishi, Chem. Commun. 46, 4438 (2010).
12) H. Okamoto, Y. Shimada, Y. Oka, A. Chainani, T. Takahashi, H. Kitagawa, T. Mitani, K. Toriumi, K. Inoue, T. Manabe and M. Yamashita, Phys. Rev. B: Condens. Matter, 54, 8438 (1996).
13) S. Takaishi, M. Takamura, T. Kajiwara, H. Miyasaka, M. Yamashita, M. Iwata, H. Matsuzaki, H. Okamoto, H. Tanaka, S. Kuroda, H. Nishikawa, H. Oshio, K. Kato and M. Takata, J. Am. Chem. Soc. 130, 12080 (2008).
14) T. Yoshida, S. Takaishi, H. Iguchi, H. Okamoto, H. Tanaka, S. Kuroda, Y. Hosomi, S. Yoshida, H. Shigekawa, T. Kojima, H. Ohtsu, M. Kawano, B. K. Breedlove, L. Guerin and M. Yamashita, Chemist. Select Commun. 2, 259 (2016).
15) A. Hazell,Acta Crystalloger.sect.C. 47, 962 (1991).
16) Y. Wakabayashi, N. Wakabayashi, M. Yamashita, T. Manabe, N. Matsushita, J. Phys. Soc. Jpn. 68, 3948 (1999).
17) M. Ishida, T. Mori, and H. Shigekawa, Phys. Rev. Lett. 83, 596 (1999).
18) H. Dai and M. Lieber, Annual Rev. Phys. Chem. 44, 237 (1993).
19) T. Nishiguchi, M. Kageshima, M. Rara-Kato and A. Kawazu, Phys. Rev. Lett. 81, 3187 (1998).
20) M. Ishida, T. Mori and H. Shigekawa, Surf. Sci. 433, 147 (1999).
21) M. Ishida, T. Mori and H. Shigekawa, Synthetic Metals 103, 2105 (1999).
22) M. Ishida, K. Hata, T. Mori, K. Nakamoto, M. Iwatsuki, R. Yoshizaki and H. Shigekawa,

Jpn. J. Appl. Phys. 36, 1294 (1997).

23) M. Yamashita, T. Ishii, H. Matsuzaka, T. Manabe, T. Kawashima, H. Okamoto, H. Kitagaza, T. Mitani, K. Marumoto, S. Kuroda, Inorg. Chem. 38, 5124 (1999).

Figure Captions

Fig. 1. Schematic structures of (a) charge density wave (CDW) and (b) Mott-Hubbard (MH) states. Arrows indicate spins. The d_{z^2} bands of Pd^{II} and Pd^{IV} in the CDW state form a conduction band and valence band, respectively, while the d_{z^2} band of Pd^{III} in the MH state splits into the unoccupied upper Hubbard band (UH) and the occupied lower Hubbard band (LH), owing to the strong interaction between electrons. E_F indicates Fermi energy.

Fig. 2. Schematic of the crystal structure of $[Pd(cptn)_2Br]Br_2$ (cptn: 1R, 2R-diaminocyclopentane).

Fig. 3. STM images of $[Pd(cptn)_2Br]Br_2$ surfaces obtained at (a) room temperature (V_s = 1.5 V, I_t = 0.08 nA) and (b) 103 K (V_s = 4.0 V, I_t = 0.1 nA).

Fig. 4. Variation in the STM images of the $[Pd(cptn)_2Br]Br_2$ surface with decreasing (a to c) and increasing (d and e) sample temperature, showing the temperature dependence of the phase transition between the CDW and MH phases. The measurement conditions (V_s, I_t) were (a) (2.0 V, 0.2 nA), (b) (3.5 V, 0.1 nA), (c) (4.0 V, 0.08 nA), (d) (3.3 V, 0.08 nA), and (e) (3.8 V, 0.08 nA). The area ratios between the CDW and MH phases shown above the STM images were obtained from the average of the STM images measured over 25 nm × 25 nm areas at different locations at each temperature. (f) Cross section along the 1D chain surrounded by the dashed rectangle in (d).

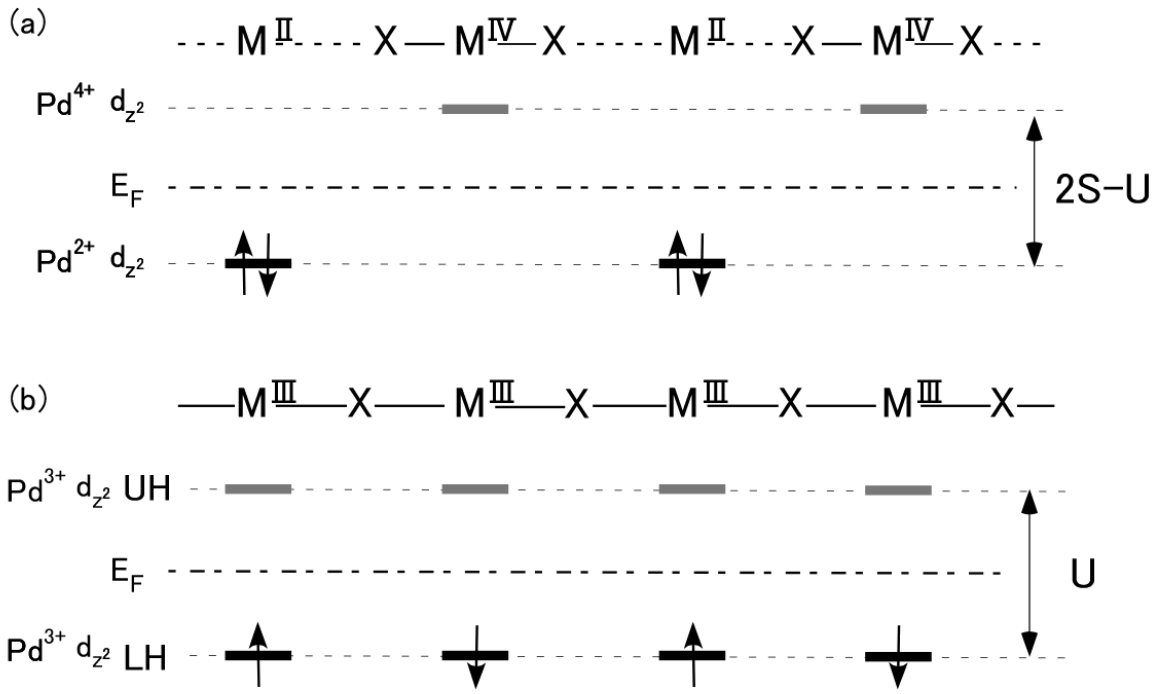
(a)
M II X M IV X M II X M IV X
Pd4+ dz2
EF
2S−U
Pd2+ dz2
(b)
M III X M III X M III X M III X
Pd3+ dz2 UH
EF
U
Pd3+ dz2 LH

Fig.1.

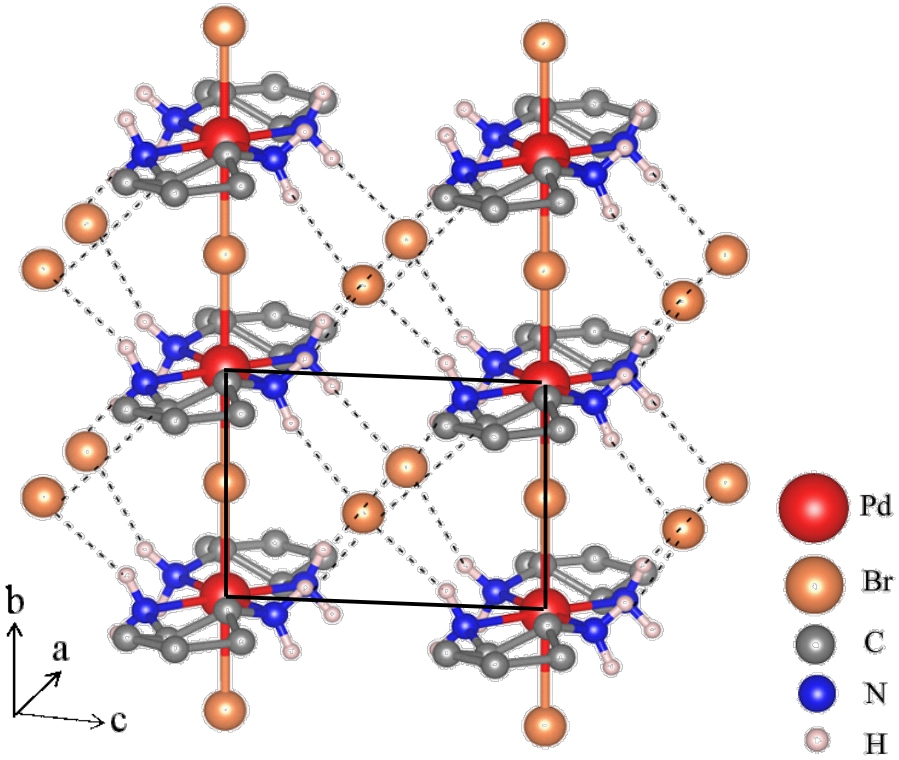

Fig.2.

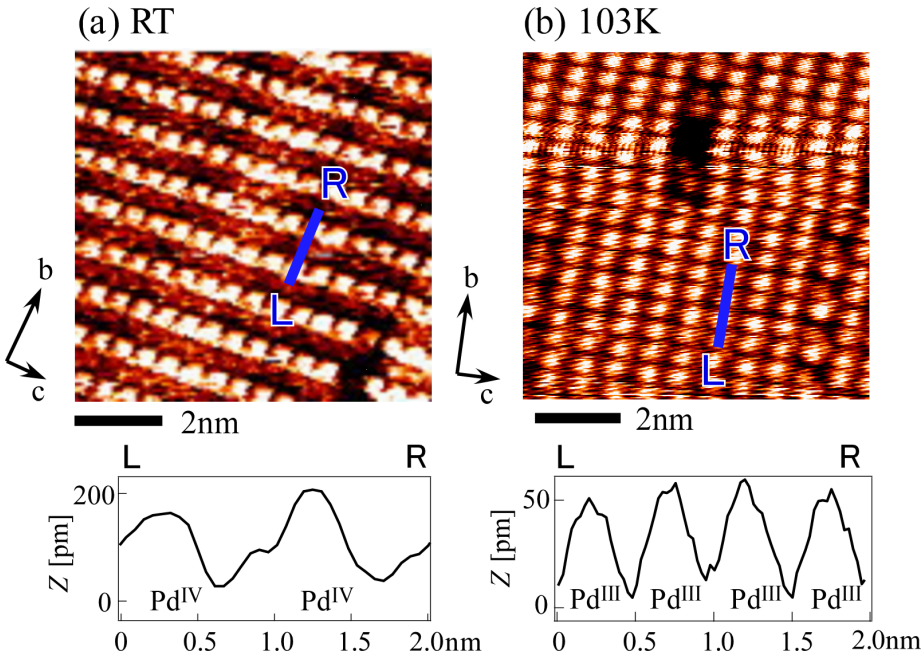
(a) RT
(b) 103K
R
L
b
c
2nm
L
R
200
0
Z [pm]
Pd^IV
Pd^IV
0
0.5
1.0
1.5
2.0nm
50
Pd^III
Pd^III
Pd^III
Pd^III

Fig.3.

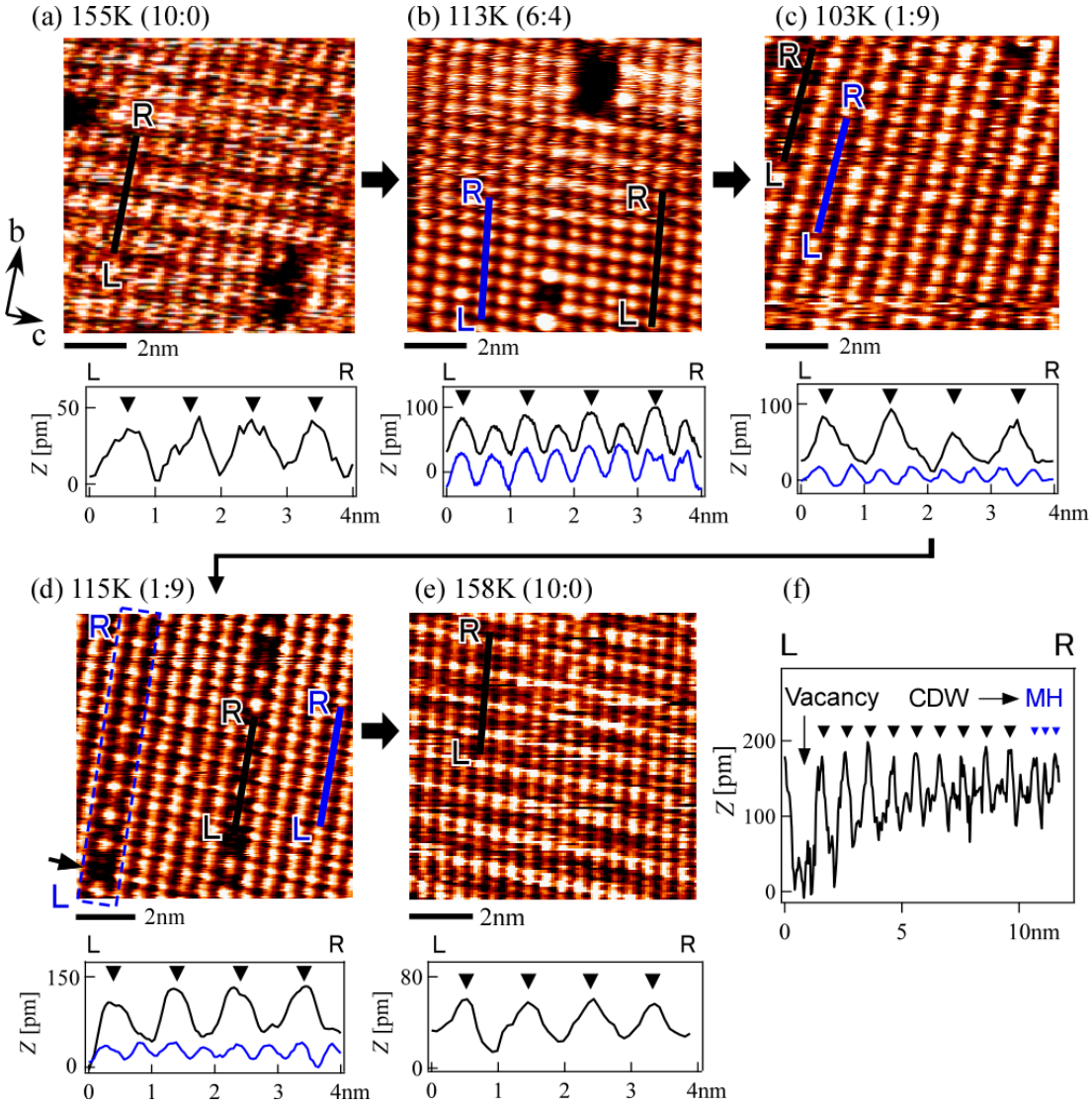
(a) 155K (10:0)
(b) 113K (6:4)
(c) 103K (1:9)
(d) 115K (1:9)
(e) 158K (10:0)
(f)
b
c
R
L
2nm
Z [pm]
4nm
Vacancy
CDW
MH
10nm

Fig.4.